Preprints of the 19th World Congress
The International Federation of Automatic Control
Cape Town, South Africa. August 24-29, 2014

Nonlinear control applied to a dc-dc power converter and the load sharing problem in a dc microgrid ⋆

Eduardo Lenz * **Daniel J. Pagano** * **Vinicius Stramosk** *

* *Department of Automation and Systems, Federal University of Santa Catarina, Florianópolis, Brazil (e-mail: {eduardo.lenz, vinicius.stramosk}@posgrad.ufsc.br, daniel.pagano@ufsc.br)*

Abstract: The purpose of this paper is to apply the Immersion & Invariance and Passivity-based Control to a dc-dc power converter driving a nonlinear load. Experimental results are shown in order to evaluate the performance of the proposed control techniques. Another goal is to find a model for a dc microgrid (load sharing problem) and to show some stability issues.

Keywords: Microgrids; Load Sharing; Constant Power Loads; Immersion & Invariance.

1. INTRODUCTION

In this work Passivity-Based Control (PBC) and the Immersion & Invariance (I&I) technique (Astolfi and Ortega (2003)) control techniques will be developed in order to drive a dc-dc power converter with a nonlinear load, which is a Constant Power Load (CPL).

The first part of this paper is basically a sequel from Lenz and Pagano (2013) with applications for a buck-type of power converter and with some experimental results for buck and boost power converters.

The second part of this paper is concerns to analyze the load sharing problem that basically appears when two or more different sources are connected to the dc link by means of electronic power converters. A simplified case of a dc microgrid with two sources (batteries) connected by bidirectional power converters and driving a CPL is shown in Fig. 1. The sources in a dc microgrid must achieve proper power sharing and, at the same time, attend for stability and dynamic performance of the system. Therefore, the designing of such systems is much more challenging than stand-alone operation of power converters because of the sources and loads interaction. Among the strategies of power sharing, the most widely used and accepted are the methods based on a droop control because of simplicity and efficiency, Guerrero et al. (2011). Moreover, the droop control essentially works by reducing the voltage reference of each source as the current increases. For more details about microgrids and droop control, see Boroyevich et al. (2010); Dragicevic et al. (2014); Lu et al. (2014). Thus, in this paper, a second objective is to develop a simplified model for a dc microgrid (load sharing problem) and to analyze the system stability.

The load characteristic of this system is presented in Fig. 2. CPLs are prone to instability due to its negative resistance feature when linearized, although this behavior is only

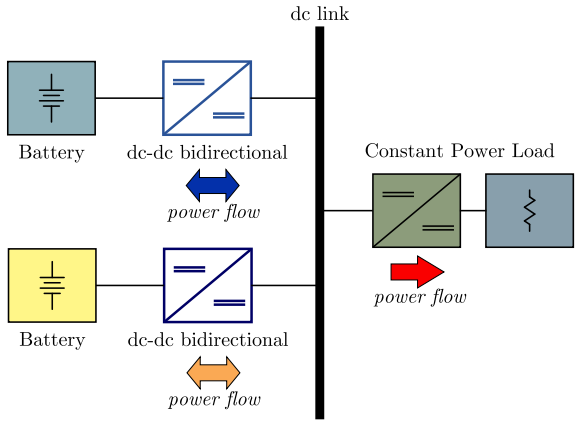

Fig. 1. The load sharing problem in a microgrid.

valid when the input voltage of the load reaches a threshold voltage (V_{th}). Before that, the load acts as a resistance for a buck type of load. For a boost type, it acts as a current source due to the limiting action of the current control. The CPL model is an instantaneous nonlinear model but any realistic load has some kind of internal dynamics. An ideal CPL can be seen as the worst-case scenario for a control system, so all our designs will be developed for such load, even if a power converter is easier to control.

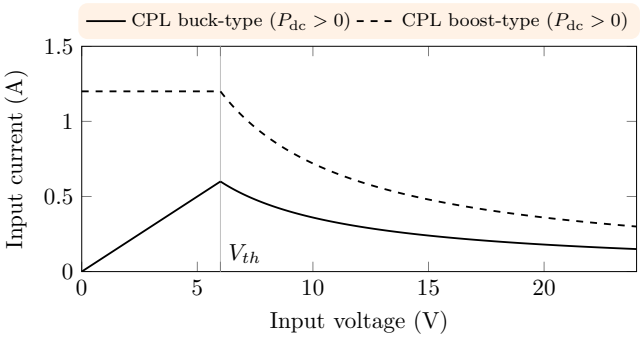

Fig. 2. Equivalent load connected to the dc link.

⋆ Project developed under the R&D Program of Tractebel Energia regulated by ANEEL.

The remainder of the article is organized as follows. The modeling of dc-dc stand-alone bidirectional power converter with a nonlinear load and the nonlinear control techniques applied to that system are presented in Sections 2 and 3, respectively. Experimental results for the case of buck and boost power converters are summarized in Section 4. Section 5 describes the modeling, stability analysis and control of load sharing in dc microgrids.

2. DC-DC BIDIRECTIONAL POWER CONVERTER

The topology of the dc-dc power converter is shown in Fig. 3. Note that this converter can operate as a buck or as a boost converter. If the output voltage is going to be controlled then the converter becomes a buck. On the other hand, if controlling the input voltage is the aim, then the converter behaves like a boost converter. The reference for input and output terminals is obviously arbitrary and our choice of reference is based on the buck converter. Much of the voltage and current control designed in the following sections can be used in the load sharing problem, or at least easily adapted to such situation. So before we are able to deal with the load sharing, we must be able to control a power converter driving a unstable load such as the CPL without any problems.

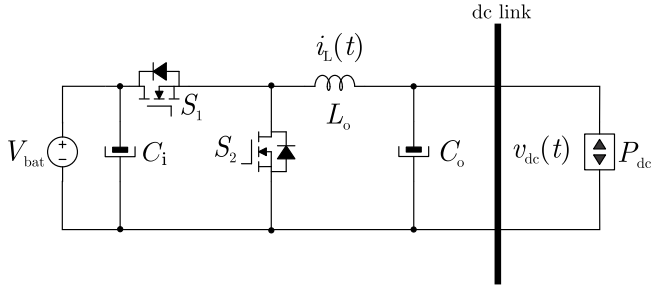

Fig. 3. Topology of the dc-dc power converter in the buck mode.

The local average model of the dc-dc power converter in the buck mode is given by

$$L_{\rm o}\frac{di_{\rm L}}{dt} = -v_{\rm dc} + V_{\rm bat}\,u \tag{1}$$

$$C_{\rm o}\frac{dv_{\rm dc}}{dt} = i_{\rm L} - \frac{P_{\rm dc}}{v_{\rm dc}} \tag{2}$$

where $i_{\rm L}$ and $v_{\rm dc}$ are the states of the system; $V_{\rm bat}$ is the battery voltage; u is the duty cycle; and $P_{\rm dc}$ is the load power. The control variable is limited to the interval $u \in [0; 1]$.

It is interesting to obtain a normalized model of the converter, thus (1) and (2) become

$$\dot{x} = -y + u \tag{3}$$

$$\dot{y} = x - \frac{p_{\rm o}}{y} \tag{4}$$

where $x = (Z_{\rm o}/V_{\rm bat})\,i_{\rm L}$; $y = v_{\rm dc}/V_{\rm bat}$; $\tau = \omega_{\rm o}t$; $p_{\rm o} = \left(Z_{\rm o}/V_{\rm bat}^2\right)P_{\rm dc}$; $Z_{\rm o} = \sqrt{L_{\rm o}/C_{\rm o}}$; and $\omega_{\rm o} = 1/\sqrt{L_{\rm o}C_{\rm o}}$. Note $\dot{x}$ and $\dot{y}$ denote the derivatives with respect to τ.

In the next sections we are going to apply some control techniques to the buck mode of operation, which will be a basic cascate control with two loops. For control techniques applied to the boost power converter see Lenz and Pagano (2013); Stramosk et al. (2013) and for the buck mode see Kwasinski and Krein (2007).

The cascade control system structure used to control the buck converter is shown in Fig. 4. A constant voltage reference ($Y_{\rm ref}$) enter the voltage loop, which generates a current reference ($X_{\rm ref}$) for the current loop.

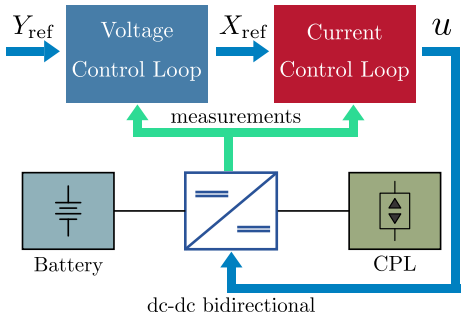

Fig. 4. Control system structure: Cascate control with two loops.

3. PASSIVITY-BASED CONTROL AND IMMERSION & INVARIANCE CONTROL

3.1 Current Control Loop (PBC)

The PBC applied to the buck converter is given by

$$\dot{x}_c = -y_c + u + \mathcal{K}_1\,(x - x_c) \tag{5}$$

$$\dot{y}_c = x_c - \frac{\hat{p}_{\rm o}}{y} + \mathcal{K}_2\,(y - y_c) \tag{6}$$

where x_c stands for the current; y_c represents the voltage; $\mathcal{K}_1$ and $\mathcal{K}_2$ are the PBC gains; and $\hat{p}_{\rm o}$ is the output power estimation.

The PBC is designed to control the inductor current; for the output voltage, the I&I will be used. Based on this information, x_c is the reference signal (it is the $X_{\rm ref}$ from Fig. 4) for the PBC and because it is a dc-dc power converter, it can be approximated to a constant reference. Therefore we can neglect its dynamics (i.e. $\dot{x}_c = 0$), and so the duty cycle is given by

$$u = y_c - \mathcal{K}_1\,(x - x_c)\,. \tag{7}$$

To estimate the output power, we can propose the following estimation error:

$$e_p = (\alpha_p + \beta_p) - p_{\rm o}$$

$$\dot{e}_p = \dot{\alpha}_p - \frac{\partial \beta_p}{\partial y}\left[x - \frac{\alpha_p + \beta_p - e_p}{y}\right]$$

where $\alpha_p + \beta_p$ is the parameter estimation. Choosing $\dot{\alpha}_p$ to simplify the estimation error dynamics, we have

$$\dot{e}_p = \frac{\partial \beta_p}{\partial y}\frac{e_p}{y} = -\kappa e_p$$

where

$$\beta_p = -\frac{1}{2}\kappa y^2.$$

The error is exponential stable (κ is the estimation gain), and now we can proceed to show that the PBC is stable:

$$\mathcal{V} = \frac{1}{2}(x - x_c)^2 + \frac{1}{2}(y - y_c)^2$$
$$\dot{\mathcal{V}} = -\mathcal{K}_1 (x - x_c)^2 - \mathcal{K}_2 (y - y_c)^2 .$$

Note that it was assumed that the parameter error was null in the Lyapunov function dynamics.

3.2 Voltage Control Loop (I&I)

The output dynamics is given by

$$\dot{y} = x - \frac{p_o}{y}. \tag{8}$$

Making the following change of variables, $w_o = \frac{1}{2}y^2$ and $p_{in} = xy$, we have

$$\dot{w}_o = p_{in} - P_o. \tag{9}$$

As $x \to x_c$, $p_{in} = x_c y$ when the PBC is operating on the steady state. If we choose $e_o = W_{ref} - w_o$ as the error signal, the error dynamics will be

$$\begin{aligned}\dot{e}_o &= -p_{in} + p_o \\ &= -K_{o1} e_o - K_{o2} \int e_o(\tau)\, d\tau.\end{aligned}$$

We can propose the following parameter estimation:

$$z = \alpha + \beta - p_o.$$

The estimation dynamics is

$$\begin{aligned}\dot{z} &= \dot{\alpha} + \frac{\partial \beta}{\partial w_o}\left[p_{in} - (\alpha + \beta - z)\right] \\ &= \frac{\partial \beta}{\partial w_o} z \\ &= -\lambda_o w_o z\end{aligned}$$

where $\beta = -\frac{1}{2}\lambda_o w_o^2$ with λ being an estimation gain. The dynamic part of the estimation is

$$\dot{\alpha} = \lambda_o w_o \left[K_{o1} e_o + K_{o2} \int e_o(\tau)\, d\tau\right],$$

therefore the input power is given by

$$\begin{aligned}p_{in} = {} & K_{o1} e_o + K_{o2} \int e_o(\tau)\, d\tau - \frac{1}{2}\lambda_o w_o^2 \\ & + \lambda_o K_{o1} \int w_o(\tau)\, e_o(\tau)\, d\tau \\ & + \lambda_o K_{o2} \int w_o(\tau) \int e_o(\xi)\, d\xi\, d\tau\end{aligned} \tag{10}$$

where ξ is the dummy variable for the time in the inner integral. Finally, the PBC reference, which is the output of the I&I, is

$$x_c = \frac{p_{in}}{y}.$$

From Fig. 4, we can see that the energy reference is just

$$W_{ref} = \frac{1}{2} Y_{ref}.$$

4. EXPERIMENTAL RESULTS

The experimental results are developed for the circuit in Fig. 3. The configuration that we have it is a dc-dc power converter driving a CPL which is another dc-dc power converter driving a linear (resistive) load. This work focus on the buck mode of operation for the dc-dc bidirectional power converter, but a boost mode is also possible with the input terminals exchanged with the output terminals. Because of that, the experimental results will be developed for both modes of operation. The system specification is given by Table 1 with the reference based on the buck mode of operation.

Table 1. dc-dc power converter specification

output voltage	12 V
input voltage	24 V
switching frequency	25 kHz
inductance	2.2 mH
output capacitance	10 μF
input capacitance	47 μF

4.1 Boost Mode

To see how the converter behaves with load changes, the signal reference for the load dc-dc converter has undergone a step. Fig. 5 shows the dc-link voltage for an increase in the output power. CH1 (orange) is the dc link voltage and CH2 (blue) is the output voltage of the CPL. For a decrease in the output power, Fig. 6 shows again the dc link voltage.

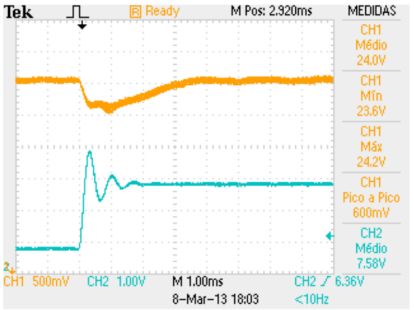

Fig. 5. dc link voltage in the boost mode (CH1 - orange) - CPL increases from 1.8 W to 3.2 W.

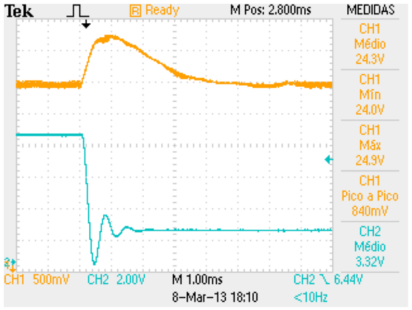

Fig. 6. dc link voltage in the boost mode (CH1 - orange) - CPL decreases from 3.2 W to 0.2 W.

4.2 Buck Mode

For the buck mode, the same situation occurs: the dc link voltage (CH4 - green) is the variable of interest; and the CPL output voltage (CH2 - blue) suffers a step in the reference signal. An increase in the output power is shown in Fig. 7, for a decrease in the output power, see Fig. 8.

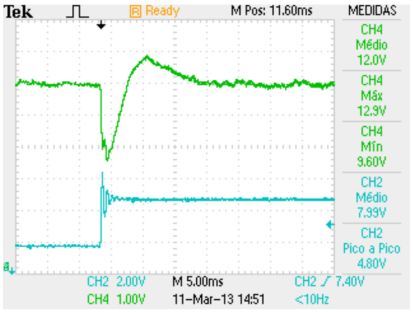

Fig. 7. dc link voltage in the buck mode (CH4 - green) - CPL increases from 3.24 W to 5.49 W.

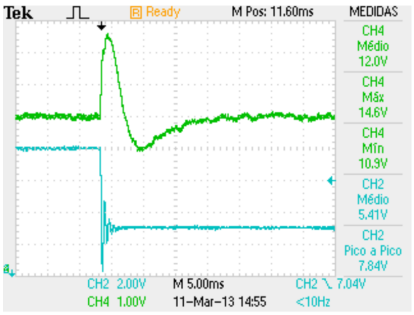

Fig. 8. dc link voltage in the buck mode (CH4 - green) - CPL decreases from 5.49 W to 2.24 W.

5. THE LOAD SHARING PROBLEM IN A DC MICROGRID

The past sections deal with the problem of a power converter driving a CPL (stand-alone operation). Now we can proceed to a more challenging problem, the load sharing between two power converters, for instance the problem in Fig. 1. We can assume that the output current of each power converter is measured, but the communication between the power converters are not fast enough to be used for the control system. This means that the control system for the first power converter does not know the current from the second power converters and vice versa.

The control structure that is aimed is a very simple one, a cascate control with basically three loops: inductor current loop; capacitor voltage loop; and an output current loop (load sharing loop). The last loop is designed assuming that the inner loops are in the steady state, therefore the power converter becomes a controlled voltage source, see Fig. 9. Note that if the load sharing loop is oscillatory or even unstable, then this modeling approach may not work, simply because those inner loops will not be constants in the steady state and the power converter may not be modeled as a simple voltage source.

The lines that connect the two power converters will be modeled as a RLC element; hence the load sharing problem can be modeled as

$$L_1 \frac{di_1}{dt} = -R_1 i_1 + V_1 - v_{\rm dc} \tag{11}$$

$$L_2 \frac{di_2}{dt} = -R_2 i_2 + V_2 - v_{\rm dc} \tag{12}$$

$$C \frac{v_{\rm dc}}{dt} = i_1 + i_2 - \frac{P_{\rm dc}}{v_{\rm dc}}. \tag{13}$$

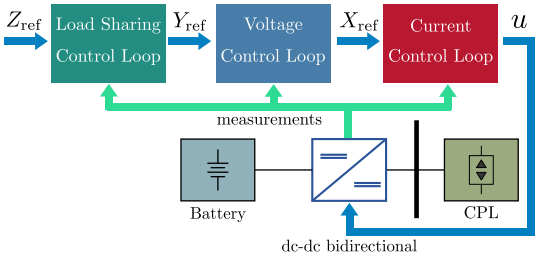

Fig. 9. Control system structure: Cascate control with three loops for each power converter connected in the microgrid.

When the system is normalized, using the same normalizing factors from Section 2, it becomes

$$\ell_1 \dot{z}_1 = -r_1 z_1 + Y_1 - y_{\rm dc}$$
$$\ell_2 \dot{z}_2 = -r_2 z_2 + Y_2 - y_{\rm dc}$$
$$c\, \dot{y}_{\rm dc} = z_1 + z_2 - p_{\rm o}/y_{\rm dc}$$

where ℓ_1 (ℓ_2) is the normalized line inductance for the first (second) power converter; r_1 (r_2) is the normalized line resistance for the first (second) power converter; c is the normalized equivalent capacitance; $p_{\rm o}$ is the normalized load power; z_1 (z_2) is the output current of the first (second) power converter; $y_{\rm dc}$ is the normalized dc link voltage; Y_1 (Y_2) is the output voltage of the first (second) power converter in the steady state and it is the control variable for this problem (it is $Y_{\rm ref}$ in Fig. 9). The only reason that we are going to use the same normalization factors from Section 2 is to match what will be done in the load sharing loop to the inner control loops. Finally, in those equations only the nonlinear part of the CPL is being shown.

The load sharing parameters are in Table 2.

Table 2. load sharing specification

rated voltages V_1, V_2	380 V
line resistance R_1	10 mΩ
line resistance R_2	30 mΩ
line inductance L_1	1 μH
line inductance L_2	3 μH
equivalent line capacitance C	1 μF
load power	1 kW - 5 kW

The equivalent circuit with the output of each power converter modeled as a voltage source can be seen in Fig. 10.

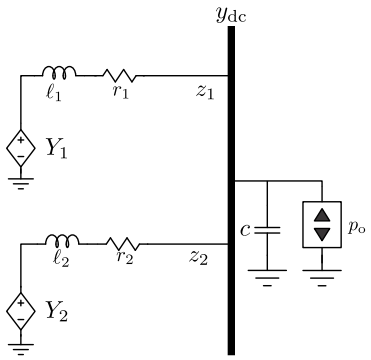

Fig. 10. Equivalent circuit of diagram in Fig. 1 showing the normalized RLC line parameters and the CPL.

Before anything else, we must define which type of microgrid is desired here. We are going to assert the presence of a central controller that has a communication link with all the power converters connected to the dc microgrid. This central controller can send a reference signal for each power converter, a reference that we can assume it is of the current-type, or at least can be transformed to a current reference. Our model can be developed based on the output power of each power converter or by their output currents. The models using currents are easier to work.

5.1 Stability Analysis

Without any load sharing control and with the voltage references $Y_1 = Y_2 = Y_{\text{ref}}$, the system has two equilibrium points, one close to Y_{ref} and another one that is close to zero, both given by the solutions of

$$Y_{\text{dc}}^2 - Y_{\text{ref}} Y_{\text{dc}} + \frac{r_1 r_2}{r_1 + r_2} p_{\text{o}} = 0 \tag{14}$$

with Y_{dc} as the equilibrium point for the dc link voltage. The equilibrium point close to zero is virtual because of the discontinuous behavior of the CPL (Fig. 2). We can focus only on the equilibrium point close to Y_{ref}.

The maximum power that can flow in this microgrid is

$$p_{\text{max}} = \frac{r_1 + r_2}{r_1 r_2} \frac{Y_{\text{ref}}^2}{4}. \tag{15}$$

We can linearize the system equations with the jacobian matrix given by

$$A = \begin{bmatrix} -\dfrac{r_1}{\ell_1} & 0 & -\dfrac{1}{\ell_1} \\ 0 & -\dfrac{r_2}{\ell_2} & -\dfrac{1}{\ell_2} \\ \dfrac{1}{c} & \dfrac{1}{c} & \dfrac{p_{\text{o}}}{Y_{\text{dc}}^2 c} \end{bmatrix}. \tag{16}$$

The characteristic equation ($\lambda^3 + a_2\lambda^2 + a_1\lambda + a_0 = 0$) has the following coefficients:

$$a_0 = \frac{r_1 + r_2 - p_{\text{o}} r_1 r_2 / Y_{\text{dc}}^2}{\ell_1 \ell_2 c} \tag{17}$$

$$a_1 = \frac{\ell_1 + \ell_2}{\ell_1 \ell_2 c} + \frac{r_1 r_2}{\ell_1 \ell_2} - \frac{p_{\text{o}}}{Y_{\text{dc}}^2 c}\left(\frac{r_1}{\ell_1} + \frac{r_2}{\ell_2}\right) \tag{18}$$

$$a_2 = \frac{r_1}{\ell_1} + \frac{r_2}{\ell_2} - \frac{p_{\text{o}}}{Y_{\text{dc}}^2 c}. \tag{19}$$

Using the Routh–Hurwitz stability criterion we can find the stability conditions ($a_0 > 0$, $a_2 > 0$ and $a_1 > a_0/a_2$). When a_1 is less than a_0/a_2, the system goes to a subcritical Hopf bifurcation (HB) and an unstable limit cycle appears (green curve in Fig.11). Another bifurcation, the Saddle Node of Periodic Orbits (SNPO), occurs when the power is decreased from the HB point. At this turning point two limit cycles appear (see Fig. 11), one unstable and the other stable, around the stable equilibrium point. The stable limit cycle is denoted by a blue curve in Fig. 11. Those results were obtained using numerical continuation techniques applied to the problem.

5.2 Droop Control

The basic loop sharing control for microgrids, the droop control, is a simple proportional control defined by

$$Y_1 = Y_{\text{ref}} + K_{\text{droop}} \left(Z_{\text{ref}} - z_1\right).$$

with Z_{ref} generated by the MGCC and defined as $Z_{\text{ref}} = p_{\text{o}}/2Y_{\text{dc}}$, since we want each power converter delivering the same amount of power.

In order to analyze the effect of this controller on the system's stability, it is only necessary to make the following changes for (17)-(19):

$$r_1 \to r_1 + K_{\text{droop}}$$
$$r_2 \to r_2 + K_{\text{droop}}.$$

Also, (14) changes to

$$Y_{\text{dc}}^2 - \left(Y_{\text{ref}} + K_{\text{droop}} Z_{\text{ref}}\right) Y_{\text{dc}} + \frac{r_1 r_2}{r_1 + r_2} p_{\text{o}} = 0.$$

The major effect that this control can have is to pospone the Hopf bifurcation by increasing the line resistances, but the maximum power, given by (15), will decrease. Besides the stability effect, if $K_{\text{droop}} > \{r_1, r_2\}$, each power converter will send almost the same amount of power to the load. A similar bifurcation diagram can be built for the case with droop control, as shown in Fig. 12.

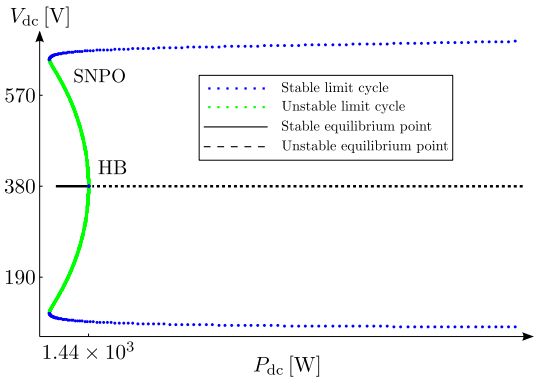

Fig. 11. Bifurcation diagram on the (P_{dc}, V_{dc})-plane with P_{dc} as the bifurcation parameter for the microgrid without a load sharing controller.

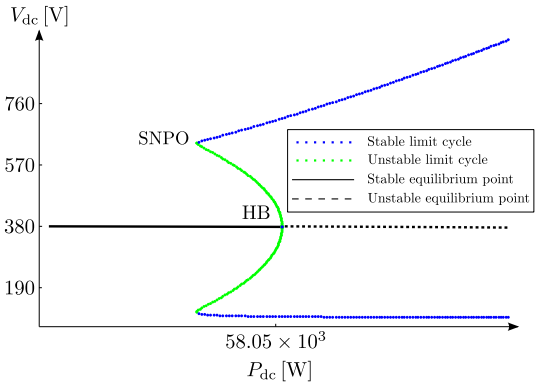

Fig. 12. Bifurcation diagram on the (P_{dc}, V_{dc})-plane with P_{dc} as the bifurcation parameter for the microgrid with droop control.

With droop control, the critical value of P_{dc} for the Hopf bifurcation went from 1.44 kW to 58.05 kW, which is a huge increase for the power flow stability in this microgrid. The only problem with this controller is that the maximum power capability is decreased because of the increment in the line resistance due to K_{droop}.

5.3 Simulation Results

The simulation was designed for the circuit in Fig. 1, including the power converter internal dynamics with a voltage and current control loop designed in a similar fashion to the one in Section 3. The power converter output currents and the dc link voltage are shown in Figs. 13 and 14, the first one without a load sharing controller and the second one with the droop control.

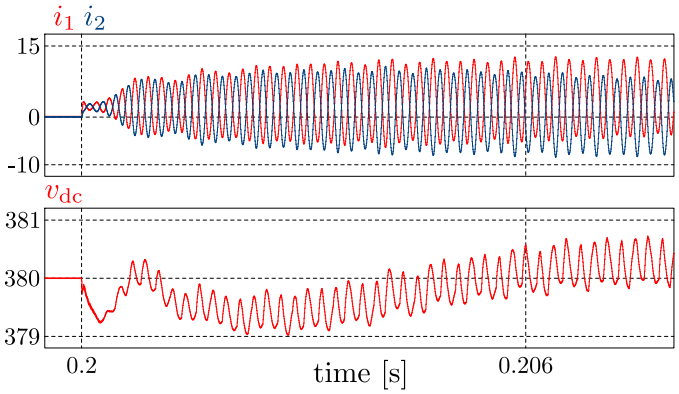

Fig. 13. Output currents (A) and dc link voltage (V) in a microgrid without a load sharing controller and with a step in the load power in 0.2 s from 100 W to 1.7 kW.

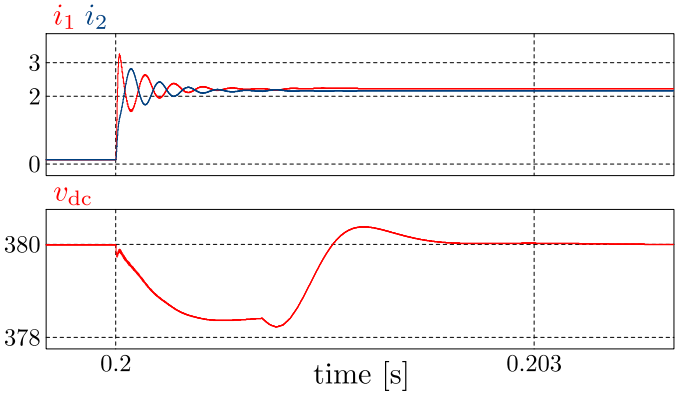

Fig. 14. Output currents (A) and dc link voltage (V) in a microgrid with droop control and with a step in the load power in 0.2 s from 100 W to 1.7 kW.

The system behavior can exhibit more complex phenomena that it was shown here, mainly because the internal dynamics of the voltage sources Y_1, Y_2 can saturate its output currents. The difference may happen when the load draws too much current from the sources.

6. CONCLUSION

From the experimental results which were developed for the first part of this paper, we can conclude that the PBC and the I&I method are interesting control solutions for the voltage regulation in a dc microgrid. In the case of the boost mode of operation, we saw that the PBC controller was very fast, but in the buck mode the PBC was clearly slower when compared to the boost mode of operation (it took over 20 ms in a step load to reach the steady state against 5 ms for the boost). Note that to ensure null error in the steady state, the I&I control technique designed for the buck converter must have a second order error dynamics contrary to a boost converter (more details in Lenz and Pagano (2013)), where a first order error dynamics is enough to accomplish null error in the steady state.

In the second part of this paper, we clearly saw that an aditional control loop is needed when power converters operates in parallel. Furthermore, without it, the system can operate with high and undesired oscillations on the currents. It is very common in the modeling of microgrids for control purposes to overlook the CPL and aproximate all the loads as linear ones; but while such approach may work, it is still not a good framework for a control system design, especially for microgrids where there are several nonlinear loads.

As to the droop control, it can make the microgrid stable for a large range in the load power. The only deficiency of the control is the difference in the output currents between the power converters when the droop gain is not substantial.

REFERENCES

Astolfi, A. and Ortega, R. (2003). Immersion and invariance: A new tool for stabilization and adaptive control of nonlinear systems. *IEEE Transactions on Automatic Control*, 48(4), 590–606.

Boroyevich, D., Cvetkovic, I., Dong, D., Burgos, R., Wang, F., and Lee, F. (2010). Future electronic power distribution systems – a contemplative view. In *12th International Conference on Optimization of Electrical and Electronic Equipment (OPTIM)*.

Dragicevic, T., Guerrero, J.M., Vasquez, J.C., and Skrlec, D. (2014). Supervisory control of an adaptive-droop regulated dc microgrid with battery management capability. *IEEE Transactions on Power Electronics*, 29(2), 695–706.

Guerrero, J.M., Vasquez, J.C., Matas, J., de Vicuña, L.G., and Castilla, M. (2011). Hierarchical control of droop-controlled ac and dc microgrids—a general approach toward standardization. *IEEE Transactions on Industrial Electronics*, 58(1), 158–172.

Kwasinski, A. and Krein, P. (2007). Stabilization of constant power loads in dc-dc converters using passivity-based control. In *29th International Telecommunications Energy Conference (INTELEC)*, 867–874.

Lenz, E. and Pagano, D.J. (2013). Nonlinear control for a bidirectional power converter in a dc microgrid. In *9th IFAC Symposium on Nonlinear Control Systems (NOLCOS)*, 359–364.

Lu, X., Guerrero, J.M., Sun, K., and Vasquez, J.C. (2014). An improved droop control method for dc microgrids based on low bandwidth communication with dc bus voltage restoration and enhanced current sharing accuracy. *IEEE Transactions on Power Electronics*, 29(4), 1800–1812.

Stramosk, V., Benadero, L., Pagano, D.J., and Ponce, E. (2013). Sliding mode control of interconnected power electronic converters in dc microgrids. In *39th Annual Conference of the IEEE Industrial Electronics Society (IECON)*.